Determination of in-plane and through-the-thickness coefficients of thermal expansion in composite angle brackets using digital image correlation

Enrique Graciani[a,*], Jesús Justo[a], Patricia Lucía Zumaquero[a]

[a] Grupo de Elasticidad y Resistencia de Materiales, Escuela Técnica Superior de Ingeniería, Universidad de Sevilla.

[*] Corresponding author. Adress: Grupo de Elasticidad y Resistencia de Materiales. Escuela Técnica Superior de Ingeniería. Camino de los Descubrimientos s/n. 41092 Sevilla, Spain.

E-mail addresses: egraciani@us.es (E. Graciani), jjusto@us.es (J. Justo), pzumaquero@us.es (P.L. Zumaquero)

Abstract

A procedure for the simultaneous determination of in-plane and through-the-thickness coefficients of thermal expansion (CTEs) in composite angle brackets is presented. Carbon fibre/epoxy samples are heated and digital image correlation is used to determine the in-plane strains and out-of-plane displacements in one side of each sample. In-plane CTEs are obtained from the average in-plane strains measured at different temperatures. Through-the-thickness CTE is obtained from the angular distortion of the samples at different temperatures, which is determined from the out-of-plane displacements. One quasi-isotropic and two unidirectional samples are used. Unidirectional samples allow the material's in-plane CTEs in orthotropic directions to be determined. Material's in-plane CTEs permit predicting an in-plane CTE value for the quasi-isotropic sample that agrees with the experimental measurements. Conversely, results obtained for the through-the-thickness CTE in all samples show a significant

dispersion. This fact is attributed to the manufacturing distortions present in the curved part of the samples.

Keywords

Thermomechanical properties; Digital Image Correlation; Anisotropy; Curved composite laminates; Manufacturing defects.

1. Introduction

Manufacturing of structural parts made of composite laminates often presents problems in fulfilling the design tolerances [1]. An accurate prediction of the final shape of composite components after the manufacturing would significantly help in reducing the costs of manufacturing and assembling of large structural parts.

Deformations undergone by composite laminates during the manufacturing process are, mainly, of chemical and thermomechanical nature, although some other aspects like tool/part interaction or lack of homogeneity in certain zones may also contribute [2-9]. The sample most commonly employed in the literature to show the distortions associated to manufacturing of composite laminates is an angle bracket like the one depicted in Fig. 1(a) [2-5,10-11]. After demoulding, the faces of the angle bracket form an angle typically smaller than that formed by the sides of the mould. This effect is usually called spring-in, spring-back or spring-forward.

While part of the distortions undergone by the composite component are irreversible, since are associated to the curing of the resin, another part is associated to the anisotropic nature of the coefficients of thermal expansion of the material and,

therefore, will change when the composite component is subjected to a temperature variation [4,12].

In the present paper, the focus is set on characterizing the thermal distortions appearing on a heated composite angle bracket. In unconstrained isotropic materials, a change in temperature induces a change in size while maintaining the shape of the part. In contrast, in orthotropic materials, like composite laminas, a change in temperature induces different changes in size in different directions. Consequently, a composite laminate, either unidirectional or formed by laminas with different orientations, typically requires a distortion of the part in order to achieve compatibility [13].

In a composite angle bracket, the main distortion caused by a homogeneous change in temperature, ΔT, is a variation $\Delta\beta$ in the initial angle bracket corner β, see Fig. 1(b).

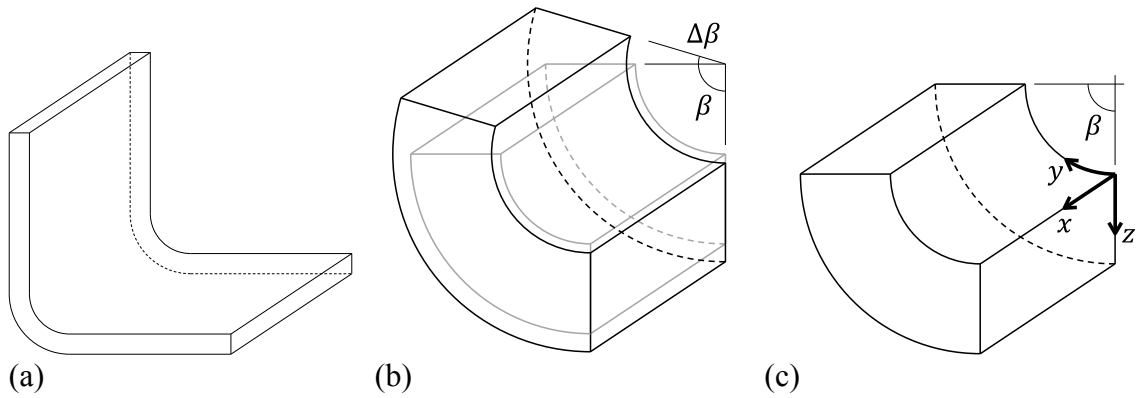(a)   (b)   (c)

Fig. 1: (a) Angle bracket, (b) thermal deformation of the angle bracket corner (gray: initial shape, black: final shape), (c) detail of the angle bracket corner.

Denoting by x the longitudinal direction, by y the circumferential direction and by z the through-the-thickness direction in the angle bracket corner, see Fig. 1(c), the unit angular variation $\Delta\beta/\beta$ can be obtained as [2]:

$$\frac{\Delta\beta}{\beta} = \frac{(\alpha_y - \alpha_z)\Delta T}{1 + \alpha_z \Delta T},$$ (1)

where α_y and α_z are, respectively, the circumferential and through-the-thickness

coefficient of thermal expansion (CTE).

The circumferential CTE can be easily and accurately determined either experimentally

[14] or analytically using Classical Laminate Theory from the stacking sequence, the

stiffness constants and the lamina's CTEs in orthotropic in-plane directions [15]

(typically denoted as α_1 for the CTE in the direction of the fibres and α_2 in the direction

perpendicular to the fibres). In comparison, very few information can be found in the

literature about the evaluation of α_z, being in many cases assumed identical to the CTE

of the laminas in the through-the-thickness direction, α_3, which, in turn, is assumed

equal to α_2 [11].

Notice that, in fact, in a composite laminate with layers having different orientations,

Classical Laminate Theory establishes that $\alpha_z \neq \alpha_3$. For example, for a quasi-isotropic

laminate [16] it holds that $\alpha_z \cong (1 + \nu_{23})\alpha_2$, with ν_{23} being the Poisson ratio.

Moreover, many authors have reported lack of homogeneity in the corner part of a

composite angle bracket, like fibre volume fraction gradients [17] or fibre

misalignments [18,19], associated to the manufacturing procedure employed.

Consequently, the apparent thermal and stiffness properties in this zone, which

significantly contribute to the deformation of the component, may be considerably

different to that of the planar parts of the component.

Measurements of $\Delta\beta/\beta$ in composite angle brackets subjected to an homogeneous

temperature change (from which the values of α_z can be derived) were presented in

[2,20,21]. In these woks, the values of $\Delta\beta/\beta$ were determined measuring the deviation of a laser beam reflected in a mirror attached to one of the angle bracket faces.

In the present paper a procedure for simultaneously measuring α_x, α_y and α_z in composite angle brackets is presented. The procedure uses digital image correlation (DIC) to determine the displacements in one of the angle bracket faces. The in-plane displacements measurements allow the in-plane CTEs, α_x and α_y, to be determined, while the out-of-plane displacements enable the calculation of $\Delta\beta$ and, with the use of (1), determining α_z. DIC has already been successfully applied to determine in-plane CTEs in polymer films [22] and composites [23,24].

Notice that, with the procedure employed, α_x and α_y are measured in the planar part of the angle bracket, while the α_z measured is in fact an apparent α_z which characterizes the thermal distortion of the angle bracket corner. The apparent α_z is evaluated using (1) and assuming that α_y in the corner and planar parts of the sample are identical, which may not be the case in the actual material. However, for practical applications, the measured in-plane CTEs will accurately account for the change in size of the component, while the measured α_z will accurately account for the change in shape.

2. Fundamentals

Thermal strains ϵ_{ij}^T of a planar orthotropic lamina, under a uniform temperature change ΔT, are given by

$$\epsilon_{ij}^T = \alpha_i \delta_{ij} \Delta T \ , \tag{2}$$

where $i,j = 1,2,3$ are the orthotropic directions (with 1 being the direction of the fibres, 2 being the in-plane direction perpendicular to the fibres and 3 being the through-the-

thickness direction), δ_{ij} is the Kronecker delta and α_i are the CTEs in orthotropic

directions.

In a typical planar composite laminate, thermal strains in each of the orthotropic laminas

can be determined, in its orthotropic co-ordinate system, using (2). However, elastic

strains should develop in order to achieve compatibility in all interfaces. In symmetric

and balanced composite laminates, thermal strains of the laminate in a global co-

ordinate system xyz, can be approximately described as those of an equivalent

homogeneous material. That is:

$$\epsilon_{kl}^T = \overline{\alpha}_k \delta_{kl} \Delta T \ , \tag{3}$$

where $k,l = x,y,z$, and $\overline{\alpha}_k$ are the average CTEs in orthotropic directions, with x being

the longitudinal in-plane direction, y being the transverse in-plane direction and z being

the through-the-thickness direction.

Finally, in a curved symmetric and balanced composite laminate, having the shape of a

hollow cylinder sector, see Fig. 1(c), with angle β, strain compatibility requires both the

presence of elastic strains and a change in shape. Consequently, in such situations,

equation (1) is only approximately satisfied. A more precise, although more

complicated, determination of the angular variation can be carried out analytically

[13,25].

3. Test campaign

In order to obtain the CTEs of a composite lamina, two unidirectional L-shaped

coupons, with stacking sequences $[0°_8]$ and $[90°_8]$ have been used. Additionally, in-

plane equivalent CTE in a quasi-isotropic sample with stacking sequence

$[0°, -45°, 45°, 90°]_S$ has been determined. In all cases the direction of the fibres in the

0° laminas follows the curvature of the sample, that is, it is parallel to the direction y shown in Fig. 1(c).

Samples were made of Hexcel AS4/8552 unidirectional prepreg laminas. A male L-shaped aluminum tool was used in the manufacturing of the samples, with a corner radius of 5 mm. Hand lay-up was carried out and bending of the layers over the tool corner was done layer by layer with the aid of nylon spatula and an air-heating device. To ensure a good compaction a first vacuum bag was used after the placement of the first four laminas. After completion of the lay-up a final vacuum was set and the material was cured in an autoclave, following the material manufacturer's specifications [26]. Coupons were cut to their final dimensions with a diamond disc saw. Nominal dimensions of the samples are: 30 mm width, 1.6 mm thickness and 60 mm × 30 mm planar faces.

The 3D stiffness matrix of an individual lamina of the material is required for the analytical calculations presented in section 4.2. Stiffness properties of the material, and stacking sequences employed are summarized in Table 1. In-plane stiffness properties E_{11}, E_{22}, G_{12} and v_{12} have been obtained following ASTM test standards [27,28]. Transverse isotropy has been assumed in the composite laminas and, consequently, out of plane E_{33}, G_{13} and v_{13} stiffness constants have been considered identical to E_{22}, G_{12} and v_{12}. Finally, v_{23} have been estimated from [29] and G_{23} has been determined using $G_{23} = E_{23}/(2 + 2v_{23})$.

Table 1. Stiffness properties of the material and stacking sequences of the samples.

Stiffness properties						Stacking sequences	
E_{11}	131.5 GPa	G_{12}	4.82 GPa	ν_{12}	0.302	"0"	$[0°_8]$
E_{22}	9.23 GPa	G_{13}	4.82 GPa	ν_{13}	0.302	"90"	$[90°_8]$
E_{33}	9.23 GPa	G_{23}	3.30 GPa	ν_{23}	0.400	"QI"	$[0°, -45°, 45°, 90°]_S$

Samples have been heated inside a calibrated convection oven (Binder FED-115) with one of their planar faces resting horizontally while the other is facing the door of the oven, see Fig. 2. The oven has been modified to let the DIC system track the coupons, substituting its opaque door by a transparent glass, which has been tempered in order to allow it to withstand the high temperatures reached during the test and to reduce the heat loses as much as possible.
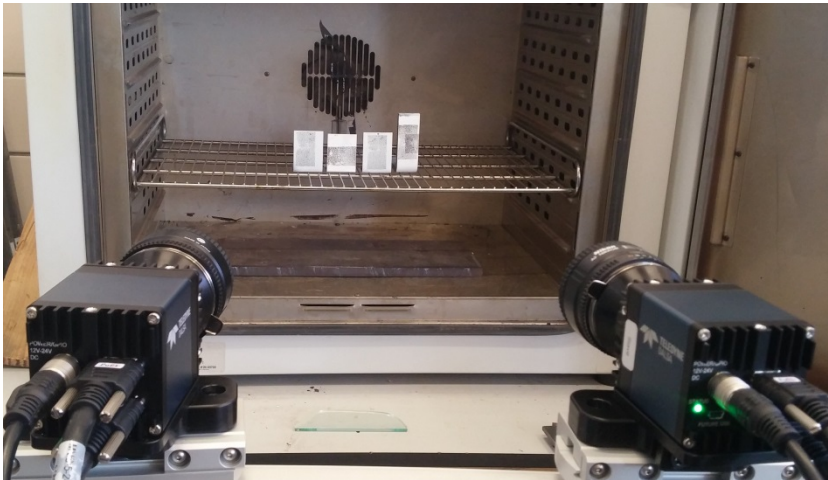

Fig. 2. Experimental setup for heating of the samples and DIC measurements.

Oven temperature has been increased up to 120℃ and measurements have been taken at intervals of approximately 30℃. Ambient temperature was 26℃. The temperature of one of the coupons has been monitored with a J-type thermocouple (placed over its

horizontal face) to verify that the temperature of the samples was stabilized prior to taking each measurement.

The displacements of the coupons have been measured with a DIC system. Two cameras have been used in order to obtain the displacements in the three spatial directions. As can be seen in Fig. 2, a 40 mm × 20 mm rectangular zone of the front face of each sample has been speckled to let the DIC software track their movements. In order to measure the displacements with high accuracy, very high resolution cameras Teledyne Imaging Falcon 2 12M (4096 x 3072 @ 58 fps) have been used.

The fourth sample that can be seen located more to the right in Fig. 2, is made of a different material and does not take part of this study.

4. Results and discussion

As mentioned above, the DIC system employed allows us to determine simultaneously the in-plane and out of plane displacements of the speckled zone in the frontal face of the samples. In the following, displacement components are denoted by u_k^P where the subscript $k = x,y,z$ indicates the component and the superscript $P = 0, 90,QI$ refers to the sample in which it is measured. The VIC-3D software employed to analyse the images is able to determine the in-plane strain components, which will be denoted as ε_{kl}^P $k,l = x,y$. Notice that direction x in the frontal face is parallel to direction x shown in Fig. 1(c), direction y is vertical and direction z is normal to the face.

As detailed in the following subsections, the in-plane material's CTEs (α_1 and α_2) have been obtained directly from the in-plane measurements in 0º and 90º coupons. The out-of-plane coefficient (α_3) has been indirectly obtained from the measurements of the out-of-plane displacements in the same coupons. Average in-plane CTE of the quasi-

isotropic laminate have been obtained analogously from the measurements of the QI coupon.

4.1. Evaluation of in plane CTEs

When the angle bracket is subjected to a uniform temperature increment, sample faces are free to deform and, consequently, uniform strains should develop. However, heterogeneities in the material introduce deviations to the ideal situation and, as a result, the experimental measurements of the strains present certain dispersion.
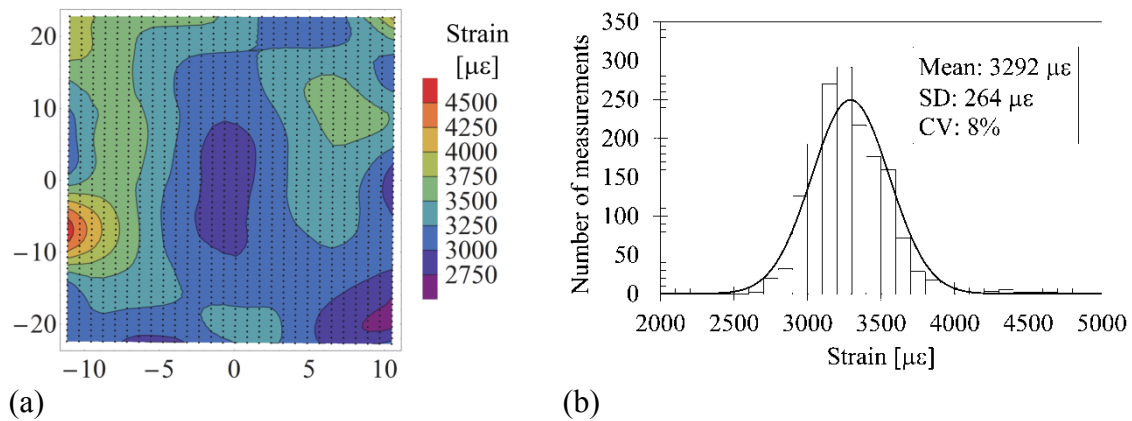
Fig. 3. Measurement of $\varepsilon_{xx}^0(x,y)$ for $T = 120°C$: (a) contour map, (b) histogram.

As an example, the colour map of Fig. 3(a) shows the results obtained in the actual measurements of ε_{xx} in the speckled region of the 0° sample. The black dots that can be seen in the image indicate the location of the points in which the DIC system provides the measurements (in each sample, the origin of the x,y coordinate system is placed in the centre of the speckled rectangle). From the individual measurements at the locations indicated in Fig. 3(a), the histogram shown in Fig. 3(b) can be constructed, where it can be clearly appreciated that measurements present a normal distribution.

10

Average values of the normal components of the measurements of in-plane stress tensor are summarized in Table 2. The uncertainty $\pm\,\delta\varepsilon$ of each measurement represents the interval in which 95% of the measurements are expected to fall, and is evaluated as:

$$\pm\,\delta\varepsilon = \frac{1.96}{\sqrt{n}}\sigma = \frac{1.96}{\sqrt{n}}\sqrt{\frac{\sum(\varepsilon_i - \bar{\varepsilon})^2}{n-1}}\,, \tag{4}$$

where ε_i denote the individual measurements, n is the number of measurements, $\bar{\varepsilon}$ is the mean value of the measurements and σ the standard deviation [30].

Table 2. Measurements of $\bar{\varepsilon}_{xx}^{P}(T)$ and $\bar{\varepsilon}_{yy}^{P}(T)$.

T [°C]	$\bar{\varepsilon}_{xx}^{0}$ [με]	$\bar{\varepsilon}_{yy}^{0}$ [με]	$\bar{\varepsilon}_{xx}^{90}$ [με]	$\bar{\varepsilon}_{yy}^{90}$ [με]	$\bar{\varepsilon}_{xx}^{QI}$ [με]	$\bar{\varepsilon}_{yy}^{QI}$ [με]
31 ±0.5	325 ±5	−25 ±5	−1 ±4	379 ±4	5 ±5	−12 ±6
60 ±0.5	1263 ±8	9 ±7	−62 ±6	1275 ±4	71 ±7	48 ±5
91 ±0.5	2439 ±12	−13 ±5	−40 ±6	2418 ±6	59 ±8	180 ±7
120 ±0.5	3292 ±13	−89 ±9	−61 ±15	3385 ±12	88 ±16	139 ±6

As detailed in the next subsections, the in-plane CTEs are obtained from the least square fit of the measurements shown in Table 2 into equation (3).

4.1.1 Unidirectional samples

Strain measurements shown in Table 2 for the 0° and the 90° samples are plotted against the temperature increment in Figs. 4(a) and (b), respectively. As can be seen, strain measurements can be accurately fitted by a straight line as defined by (3). The slope of the fitted line yields the value of the corresponding CTE.
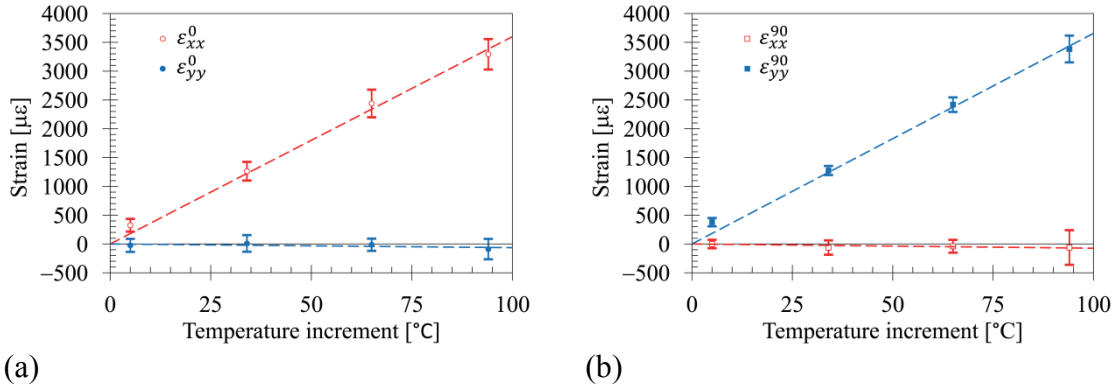
Fig. 4. Determination of the in plane CTEs by best linear fit from strain measurements: (a) 0° sample, (b) 90° sample.

Measured values of the CTEs are summarized in Table 3. In which the uncertainty $\pm \delta\alpha$ of each measurement represents the interval in which 95% of the measurements are expected to fall. For the sake of simplicity, the uncertainties of the four measurements being fitted are neglected in the determination of the uncertainty of the fitted line slope [30].

Table 3. Measurements of α_{xx}^0, α_{yy}^0, α_{xx}^{90}, α_{yy}^{90}, α_1 and α_2.

α_{xx}^0 [µε/°C]	α_{yy}^0 [µε/°C]	α_{xx}^{90} [µε/°C]	α_{yy}^{90} [µε/°C]	α_1 [µε/°C]	α_2 [µε/°C]
36.0 ±1.9	−0.6 ±0.5	−0.7 ±0.4	37 ±2	−0.7 ±0.3	36.3 ±1.4

Since unidirectional laminates are considered, it should be noticed that α_{xx}^0 and α_{yy}^{90} correspond to material's CTE α_2, while α_{yy}^0 and α_{xx}^{90} correspond to material's CTE α_1. As can be seen in Table 3, results of the two samples show an excellent agreement. Fitting together the eight strain measurements corresponding to each of the material's CTE, the results shown in Table 3 are obtained for α_1 and α_2.

4.1.2 Multidirectional laminate

Following an analogous procedure to that described in the previous section, the in-plane CTEs of the quasi-isotropic laminate of the QI sample is determined. Strain measurements $\overline{\varepsilon}_{xx}^{QI}$ and $\overline{\varepsilon}_{yy}^{QI}$ shown in Table 2 for the QI sample are plotted against the temperature increment in Figs. 5(a) and (b), respectively. Notice that the same scale employed in the plots shown Fig. 4 is employed in the plots shown Fig. 5 to avoid magnification of the uncertainties. Least squares best fit lines are represented in the plots shown Fig. 5 as discontinuous lines. As can be seen, strain measurements of QI sample can be accurately fitted by a straight line, as defined by (3). The slope of the fitted line yields the value of the corresponding CTE.
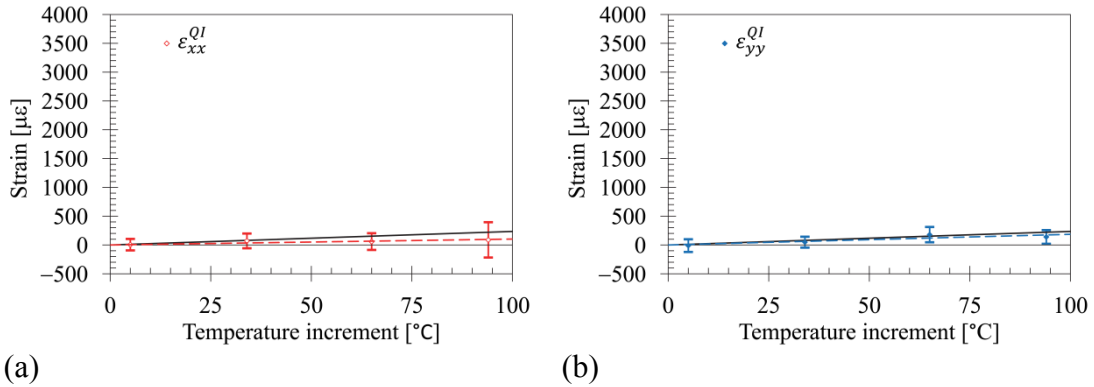

(a)   (b)

Fig. 5. Determination of the in plane CTEs by best linear fit from strain measurements in QI sample: (a) α_{xx}^{QI}, (b) α_{yy}^{QI}.

The average in-plane CTE of the QI sample can be also determined analytically, using Classical Laminate Theory, from the stiffness properties shown in Table 1 and the values of α_1 and α_2 determined in section 4.1.1 [16]. Neglecting the uncertainties of the stiffness properties, a value of $\overline{\alpha}_{QI} = (2.4 \pm 0.3)$ µε/°C is obtained. Introducing $\overline{\alpha}_{xx}^{QI} =$

$\overline{\alpha}_{yy}^{QI} = \overline{\alpha}_{QI}$ into (3) yields the solid lines shown in Fig. 5(a) and (b) which, as can be

seen, show a good agreement with experimental measurements, passing through the

confidence interval of all measurements in the two plots.

Experimental measurements of average in-plane CTE of the quasi-isotropic laminate of

the QI sample can be obtained from the slope of the least squares linear fit (shown as

discontinuous lines in Fig. 5), yielding the following results: $\alpha_{xx}^{QI} = (1.0 \pm 0.4)$ µε/°C

and $\alpha_{yy}^{QI} = (1.8 \pm 0.7)$ µε/°C . As can be seen both average in-plane CTE are very

similar and slightly below the theoretical value $\overline{\alpha}_{QI}$, derived from in-plane material's

CTEs. Deviations may be associated to slight errors in fibre orientation introduced in

the hand lay-up of the samples.

4.2. Evaluation of through-the-thickness CTE in the curved region

The apparent through-the-thickness CTE in the curved region of the sample can be

determined using (1), which, for small values of α_z, can be simplified as [31]:

$$\frac{\Delta\beta}{\beta} \cong - (\alpha_z - \alpha_y)\Delta T. \tag{5}$$

Notice also the rearrangement in signs between (1) and (5) made for clarifying

purposes. As detailed below, the angle formed by the sample faces, given by $(\pi - \beta)$,

increases in all cases when the samples are heated. Consequently, the angular variation

of the angle bracket corner $\Delta\beta$ is negative when ΔT is positive and, therefore, $\alpha_z > \alpha_y$ in
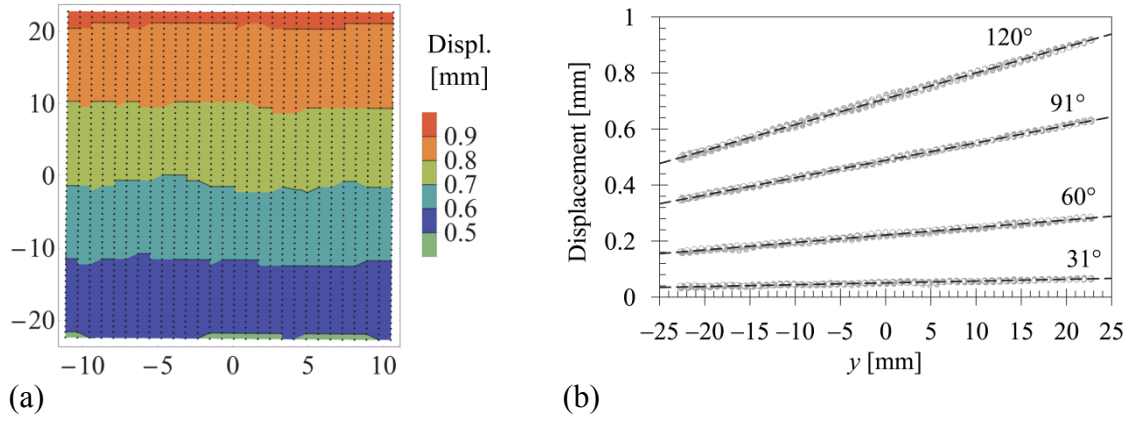
all samples.

Fig. 6. Measurement of $u_z^0(x,y)$ in 0° sample: (a) contour map at $T = 120°C$, (b) determination of $\Delta\beta$ by best linear fit from displacement measurements.

To determine the angular distortion of the sample, the normal component of the displacements is measured in the speckled zone of the frontal face of the samples. As an example, the contour shown in Fig. 6(a) shows the results obtained in the measurements of u_z in the speckled region of the 0° sample.

It can be clearly appreciated in Fig. 6(a) that horizontal bands, of approximately constant width, are formed, as correspond to a small rotation of the face, which causes normal displacements to behave as:

$$u_z^P(x,y,T) \cong u_{zo}^P(T) - \tan\left(\Delta\beta^P(T)\right) y \ . \tag{6}$$

From the individual measurements (at all temperatures) at the locations indicated in Fig. 6(a), the graph shown in Fig. 6(b) can be constructed, where it can be clearly appreciated that measurements are very accurately fitted by a straight line, with its slope increasing with the temperature increment.

Table 4. Measurements of $\Delta\beta^P(T)$.

Temperature	(31 ±0.5)°C	(60 ±0.5)°C	(91 ±0.5)°C	(120 ±0.5)°C
$\Delta\beta^0$ [·10^{-3}]	−36.9° ±0.5°	−153.2° ±0.7°	−355.1° ±0.6°	−529.6° ±1.1°
$\Delta\beta^{90}$ [·10^{-3}]	30.0° ±0.6°	−42.6° ±0.9°	−302.6° ±1.5°	−438.3° ±1.8°
$\Delta\beta^{QI}$ [·10^{-3}]	−46.7° ±0.6°	−187.3° ±0.7°	−479.2° ±0.8°	−726.2° ±1.0°

Measurements of the angular distortion suffered by the sample at each temperature have been obtained by least square fit of the individual measurements in each sample. Results obtained are summarized in Table 4.
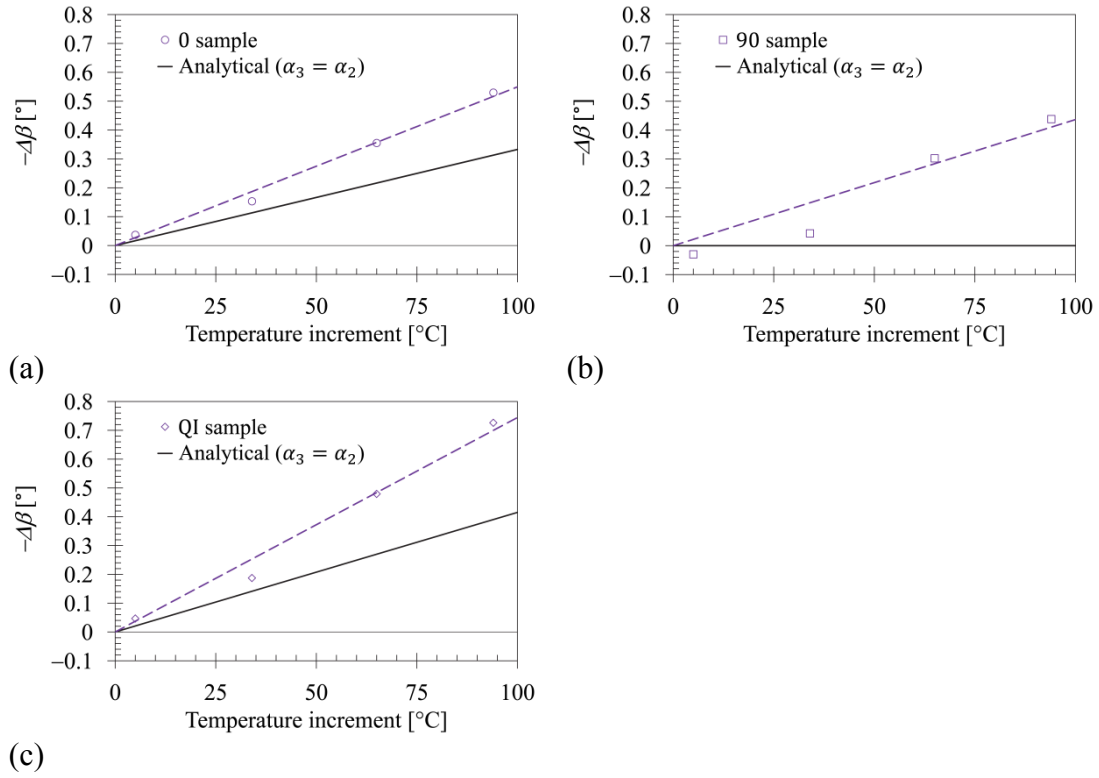

(a)

(b)

(c)

Fig. 7. Determination of $(\alpha_{zz}^P - \alpha_{yy}^P)$ by best linear fit from $\Delta\beta(T)$: (a) 0 sample, (b) 90 sample, (c) QI sample.

Measurements of the angular distortion shown in Table 4 are plotted against temperature increment ΔT in Fig. 7(a), (b) and (c), corresponding to 0, 90 and QI samples, respectively. As can be seen, in all cases, a reasonably linear dependency of $\Delta\beta^P$ with ΔT is observed, as defined by (5). Notice that $-\Delta\beta$ is used in the vertical axis in the plots shown in Fig. 7.

The value of $(\alpha_{zz}^P - \alpha_{yy}^P)$ in each sample can be obtained from the slope of the least squares linear fit of the data shown in Table 4. Best fit lines are shown as discontinuous lines in Fig. 7. Considering that the initial angle is $\beta = 90°$ in all samples, the values of $(\alpha_{zz}^P - \alpha_{yy}^P)$ shown in Table 5 are obtained.

Table 5. Measurements of $(\alpha_{zz}^P - \alpha_{yy}^P)$ and α_{zz}^P.

$\alpha_{zz}^0 - \alpha_{yy}^0$ [$\mu\varepsilon$/°C]	$\alpha_{zz}^{90} - \alpha_{yy}^{90}$ [$\mu\varepsilon$/°C]	$\alpha_{zz}^{QI} - \alpha_{yy}^{QI}$ [$\mu\varepsilon$/°C]	α_{zz}^0 [$\mu\varepsilon$/°C]	α_{zz}^{90} [$\mu\varepsilon$/°C]	α_{zz}^{QI} [$\mu\varepsilon$/°C]
61 ±5	48 ±16	83 ±9	60 ±5	85 ±16	85 ±9

Considering that α_{yy}^P in the curved zone of each sample is equal to the α_{yy}^P measured in the planar faces (shown in the previous section), the values for α_{zz}^P in the curved zone of each sample shown in Table 5 are obtained. As can be seen, results for α_{zz}^{90} and α_{zz}^{QI} are almost coincident and significantly higher than α_{zz}^0. Moreover, measured values of α_z in all cases are not consistent with the typical hypothesis that assumes $\alpha_2 = \alpha_3$. This fact can be clearly seen comparing the actual measurements of $\Delta\beta^P$ in Fig. 7 with the analytical predictions (shown as a thick line in the plots) obtained using in all samples the material properties shown in Table 1, the in-plane CTEs shown in Table 3 and

assuming $\alpha_2 = \alpha_3$. Analytical calculations have been carried out using the solution

presented in [25] and validated with finite element models with solid elements.

5. Concluding remarks

A procedure for the simultaneous determination of in-plane, α_x and α_y, and through-

the-thickness, α_z, CTEs in composite angle brackets has been presented.

To this end, L-shaped samples have been heated in an oven and DIC has been used to

determine the in-plane strains and out-of-plane displacements in one of the faces of each

sample. In-plane CTEs have been directly obtained from the best linear fit of the

average in-plane strains measured at different temperatures. Through-the-thickness CTE

have been indirectly obtained from the best linear fit of the angular distortion of the

samples at different temperatures, which, in turn, have been obtained by best linear fit

from the out-of-plane displacements.

Results obtained for in-plane CTEs in unidirectional samples, with $[0°_8]$ and $[90°_8]$

stacking sequences, show a very good agreement between each other, and allow the in-

plane material's CTEs α_1 and α_2 to be determined. Results obtained for the average in-

plane CTE in a quasi-isotropic sample, with $[0°, -45°, 45°, 90°]_S$ stacking sequence, are

also in a reasonably good agreement with the previously determined material's in-plane

CTEs.

Results obtained for the through-the-thickness CTE in all samples are significantly

higher than those predicted by the hypothesis of transversal isotropy typically carried

out in composite laminas. Moreover, the through-the-thickness CTE obtained in the [

$0°_8]$ sample is substantially smaller than those obtained in the $[90°_8]$ and

$[0°, -45°, 45°, 90°]_S$ samples.

These disagreements were expected and are not associated to the technique used for the measurements, but to the fact that the angular distortion is caused by the anisotropic behaviour of the material in the corner of the angle bracket sample and that, in this zone, the fibres are wrinkled as a result of folding the prepregs during manufacturing. Different manufacturing procedures will produce different alterations to the material in the angle bracket corner in comparison with its planar parts: thickness changes, misalignments of the fibres, fibre volume fraction gradients, etc. Consequently, to properly characterize the thermal distortion of a component, an appropriate apparent value of the through-the-thickness CTE has to be determined.

Aknowledgements

References

[1] I. Baran, K. Cinar, N. Ersoy, R. Akkerman, J.H. Hattel, A Review on the Mechanical Modeling of Composite Manufacturing Processes, Arch. Comput. Methods Eng. 24 (2017) 365–395. https://doi.org/10.1007/s11831-016-9167-2.

[2] D.W. Radford, R.J. Diefendorf, Shape Instabilities in Composites Resulting from Laminate Anisotropy, J. Reinf. Plast. Compos. 12 (1993) 58-75.

[3] C.K. Huang, S.Y. Yang, Study on Accuracy of Angled Advanced Composite Tools, Mater. Manuf. Processes. 12 (1997) 473-486. https://doi.org/10.1080/10426919708935158.

[4] D.W. Radford, T.S. Rennick, Separating sources of manufacturing distortion in laminated composites, J. Reinf. Plast. Compos. 19(8) (2000) 621-641. https://doi.org/10.1177/073168440001900802.

[5] J.M. Svanberg, J.A. Holmberg, An experimental investigation on mechanisms for manufacturing induced shape distortions in homogeneous and balanced laminates,

Composites Part A. 32 (2001) 827-838. https://doi.org/10.1016/S1359-835X(00)00173-1.

[6] G. Fernlund, N. Rahman, R. Courdji, M. Bresslauer, A. Poursartip, K. Willden, K. Nelson, Experimental and numerical study of the effect of cure cycle, tool surface, geometry, and lay-up on the dimensional fidelity of autoclave-processed composite parts, Composites Part A. 33 (2002) 341-351. https://doi.org/10.1016/S1359-835X(01)00123-3.

[7] M.R. Wisnom, M. Gigliotti, N. Ersoy, M. Campbell, K.D. Potter, Mechanisms generating residual stresses and distortion during manufacture of polymer–matrix composite structures, Composites Part A. 37 (2006) 522–529. https://doi.org/10.1016/j.compositesa.2005.05.019.

[8] N. Ersoy, T. Garstka, K. Potter, M.R. Wisnom, D. Porter, G. Stringer, Modelling of the spring-in phenomenon in curved parts made of a thermosetting composite, Composites Part A. 41 (2010) 410–418. https://doi.org/10.1016/j.compositesa.2009.11.008.

[9] J. Lian, Z. Xu, X.J. Ruan, Analysis and control of cured deformation of fiber-reinforced thermosetting composites: a review, J. Zhejiang Univ. Sci. A. 20 (2019) 311-333. https://doi.org/10.1631/jzus.A1800565.

[10] E. Kappel, D. Stefaniak, C. Hühne, Process distortions in prepreg manufacturing – An experimental study on CFRP L-profiles, Compos. Struct.106 (2013) 615–625. https://doi.org/10.1016/j.compstruct.2013.07.020.

[11] E. Hörberg, T. Nyman, M. Åkermo, S. Hallström, Thickness effect on spring-in of prepreg composite L-profiles – An experimental study, Compos. Struct. 209 (2019) 499-507. https://doi.org/10.1016/j.compstruct.2018.10.090.

[12] D.W. Radford, Balancing Mechanisms of Distortion to Yield Distortion-free/Shape Stable Composites, J. Reinf. Plast. Compos. 29 (2010) 1875-1892. https://doi.org/10.1177/0731684409340707.

[13] A.J.M. Spencer, P. Watson, T.G. Rogers, Mathematical analysis of the springback effect in laminated thermoplastic channel sections, Compos. Manuf. 2 (1991) 253-258. https://doi.org/10.1016/0956-7143(91)90147-9.

[14] R.R. Johnson, M.H. Kural, G.B. Mackey, Thermal expansion properties of composite materials, NASA Contractor Report 165632, Langley Research Center, Hampton, US, 1981.

[15] A.K. Noor, L.H. Tenek, Stiffness and thermoelastic coefficients for composite laminates, Compos. Struct. 21 (1992) 57-66. https://doi.org/10.1016/0263-8223(92)90080-V.

[16] R. Akkerman, On the properties of quasi-isotropic laminates, Composites Part B. 33 (2002) 133-140. https://doi.org/10.1016/S1359-8368(02)00002-1.

[17] D.W. Radford, Volume fraction gradient induced warpage in curved composite plates, Compos. Eng. 5 (1995) 923-934. https://doi.org/10.1016/0961-9526(95)00033-J.

[18] P. Kim, R. Phillips, S. Toll, J.A. Månson, The dimensional stability of composite laminates: sensitivity to gradients in fibre content and misalignment, in: B.

Nicquevert, C. Hauviller (eds.), International Workshop on Advanced Materials for High Precision Detectors, CERN, Geneve, 1994, pp. 119-127.

[19] P. Zumaquero, J. Justo, E. Graciani, On the thickness dependence of ILTS in curved composite laminates, Key Eng. Mater. 774 (2018) 523-528. https://doi.org/10.4028/www.scientific.net/KEM.774.523.

[20] T. Garstka, Separation of process induced distortions in curved composite laminates, PhD Thesis, University of Bristol, 2005.

[21] A. Salomi, T. Garstka, K. Potter, A. Greco, A. Maffezzoli, Spring-in angle as molding distortion for thermoplastic matrix composite, Compos. Sci. Technol. 68 (2008) 3047–3054. https://doi.org/10.1016/j.compscitech.2008.06.024.

[22] B. Pang, H.M. Xie, T. Hua, A. Anand, Measurement of coefficient of thermal expansion of films using digital image correlation method, Polym. Test. 28 (2009) 75–83. https://doi.org/10.1016/j.polymertesting.2008.11.004.

[23] C. Flament, M. Salvia, B. Berthel, G. Crosland, Digital image correlation applied to thermal expansion of composites. In: ICCM International Conferences on Composite Materials (ICCM-19), Montreal, Canada, 2013.

[24] Y.L. Dong, Z.Y. Zhang, B. Pan, High-throughput, high-accuracy determination of coefficient of thermal expansion of carbon fibre–epoxy composites using digital image correlation, Strain, 54:e12259 (2018). https://doi.org/10.1111/str.12259.

[25] J.M. González-Cantero, 3D analytical model for evaluating stresses in curved aerostructural composite laminates. Monograph ECSE2016-1. Airbus Group Chair of Aeronautical Studies, University of Seville, 2016.

[26] HexTow AS4 Carbon Fiber, Hexcel Product Data Sheet, Hexcel Coorporation, 2018. http://www.hexcel.com/user_area/content_media/raw/AS4_HexTow_DataSheet.pdf

[27] ASTM D3039 / D3039M-17, Standard Test Method for Tensile Properties of Polymer Matrix Composite Materials, ASTM International, West Conshohocken, US, 2017. https://doi.org/10.1520/D3039_D3039M-17.

[28] ASTM D3518 / D3518M-18, Standard Test Method for In-Plane Shear Response of Polymer Matrix Composite Materials by Tensile Test of a ±45° Laminate, ASTM International, West Conshohocken, US, 2018. https://doi.org/10.1520/D3518_D3518M-18..

[29] P.D. Soden, M.J. Hinton, A.S. Kaddour, Lamina properties, lay-up configurations and loading conditions for a range of fibre-reinforced composite laminates, Compos. Sci. Technol. 58 (1998) 1011-1022. https://doi.org/10.1016/S0266-3538(98)00078-5.

[30] J.R. Taylor, An introduction to error analysis. The study of uncertainties in physical measurements, second ed., University Science Books, Sausalito, 1997.

[31] J.M. O'Neill, T.G. Rogers, A.J.M. Spencer, Thermally induced distortions in the moulding of laminated channel sections, Math. Engrg. Indust. 2 (1988) 65-72.